RSC Advances

ROYAL SOCIETY OF CHEMISTRY

www.rsc.org/advances

RSC Advances

RSCPublishing

ARTICLE

A simple approach to prepare nickel hydroxide nanosheets for enhanced pseudocapacitive performance

Cite this: DOI: 10.1039/xoxxoooooox

Received ooth January 2012,
Accepted ooth January 2012

DOI: 10.1039/xoxxoooooox

www.rsc.org/

Anjon Kumar Mondal[*1], Dawei Su[1,2], Shuangqiang Chen[1], Bing Sun[1], Kefei Li[1] and Guoxiu Wang[*1]

Nickel hydroxide nanosheets were synthesized by a simple microwave assisted heating method and investigated as electrochemical pseudo-capacitive materials for supercapacitors. The crystalline structure and morphology of the as-obtained $Ni(OH)_2$ nanosheets were characterized by X-ray diffraction, nitrogen adsorption-desorption isotherms, field emission scanning electron microscopy and transmission electron microscopy. The electrochemical properties of the $Ni(OH)_2$ nanosheets were evaluated by cyclic voltammetry and chronopotentiometry technology, respectively in 2 M KOH solution. Nickel hydroxide nanosheet electrode shows a maximum specific capacitance of 2570 F g^{-1} at the current density of 5 A g^{-1} and exhibits superior cycling stability. These results suggest its potential application as electrode material for supercapacitors.

1. Introduction

Electrical energy storage and conversion from alternative energy sources have been attracting more attention due to the rising demand for energy and growing concerns about air pollution and global warming. In the recent developments of different efficient energy storage devices, supercapacitors are among the promising next-generation most investigated electrochemical power sources which offer extremely high power density, fast energy delivery, and long life cycling behaviour.[1-4] Supercapacitors are playing very important roles as energy buffers and uninterruptable power sources for hybrid electric vehicles and short-term power sources for mobile electronic devices.[5,6] On the basis of different charge storage mechanisms and the use of electrode materials, supercapacitors are divided into electrical double-layer capacitors (EDLC) and pseudocapacitors. EDLCs are usually based on the charge separation at the electrode/electrolyte interface while the pseudocapacitors involve reversible faradic redox reactions on the surface of electroactive materials.[7,8] In general, the energy density based on pseudo-faradic process is usually many times greater than that of EDLC.[9,10] Since surface properties play vital role in charge storage mechanisms, an active electrode material with improved surface properties and high capacitive performance is essential to develop an advanced supercapacitor device.[11-13]

As inexpensive and low toxic energy storage materials metal oxides and hydroxides are interesting for electrochemical capacitor applications. Although the ruthenium oxide-based supercapacitors exhibit much higher specific capacitance and better electrochemical stability, the high material cost has limited it from commercialization.[14] Many effort to date has been aimed for alternative low cost electrode materials with good capacitive properties, such as Co_3O_4,[15] MnO_2,[16,17] NiO,[18] and $Co(OH)_2$.[19] In recent years, $Ni(OH)_2$, an active transition metal hydroxide has received an increasing scientific and technological attention because it is extensively used as the electrode material in nickel-based alkaline secondary batteries such as nickel-metal hydride (Ni-MH), nickel-iron (Ni-Fe), nickel-zinc (Ni-Zn), and nickel-cadmium (Ni-Cd).[20-23] In view of its superior theoretical electrochemical properties, relatively low cost, and well-defined electrochemical redox activity, $Ni(OH)_2$ is also an attractive alternative electrode material for supercapacitors.[24-30] It is well-known that nickel hydroxide has two polymorphs: α-$Ni(OH)_2$ and β-$Ni(OH)_2$.[31,32] Both α and β-$Ni(OH)_2$ with various structures and morphologies have been synthesized, such as nanoparticles,[33] nanoflakes,[34] nanowires,[35] nanosheets[36] and nano/microspheres[37,38] using different methods. The electrochemical tests suggest that the performance of $Ni(OH)_2$ is directly affected by both its size and morphology. These improvements are ascribed to the enhanced specific surface area, first redox reaction and shorten diffusion path in the solid phase.

Among the different processing technologies being adopted for the synthesis of materials, the microwave processing has drawn much attention owing to its inherent advantages, including short heating time and homogeneous thermal transmission.[39,40] Microwave method does not produce major thermal gradients and also involve accelerated kinetics that can lead to produce material with uniform sizes and high purity.[41] In the present work, we report a simple and large-scale production strategy for the synthesis of $Ni(OH)_2$ nanosheets by a microwave heating method and investigated its electrochemical performances for supercapacitors.

2. Experimental

2.1. Synthesis of $Ni(OH)_2$ nanosheets

In the typical synthesis of $Ni(OH)_2$ nanosheets, 0.4 g of $Ni(NO_3)_2 \cdot 6H_2O$ and 0.165 g urea (molar ratio: 1:2) were dissolved in 15 ml of de-ionized (DI) water. 20 ml ethylene glycol (EG) was added into the above solution and stirred the solution for 2 h to form transparent solution. The final solution was then heated to 140 ^oC for 30 min in a microwave synthesizer (Model: NOVA-II), then allowed to cool to room temperature. The material was centrifuged, rinsed with DI water and absolute ethanol several times to remove soluble impurities. The precipitate was dried in an oven overnight at 60 ^oC.

2.2. Structure characterization

The crystallographic phases of as-synthesized $Ni(OH)_2$ nanosheets were investigated using the GBC MMA X-ray diffractometer (λ = 0.15405 nm). The specific surface area and the porosity distributions were calculated using Brunauer-Emmett-Teller (BET) nitrogen adsorption-desorption isotherms and Barrett-Joyner-Halenda (BJH) method, respectively by using a Micromeritics 3 Flex^{TM} surface characterization analyzer at 77 K. Thermogravimetric analysis (TGA) was carried out on a 2960 SDT thermal analyzer with a heating rate of 10 ^oC min^{-1} from room temperature to 700 ^oC in air. AFM measurements were performed on Dimension 3100 SPM with a tapping mode. The morphology and structure of the sample were examined by field emission scanning electron microscopy (FESEM, Zeiss Supra 55VP) and transmission electron microscopy (TEM, JEOL 2011 TEM facility).

2.3. Fabrication of electrodes and electrochemical measurements

The working electrodes were fabricated by mixing 80 wt % of as-synthesized $Ni(OH)_2$ nanosheets as an active material with 15 wt % acetylene black and 5 wt % polyvinylidene fluoride as conducting material and binder, respectively. A small amount of N-methyl-2-pyrrolidinone was added to the mixture to form slurry. The slurry was coated (area of coating: 1 cm^2) on a pre-treated Ni foam for electrical conductivity and vacuum-dried at 100 ^oC overnight. Cyclic voltammetry (CV) and chronopotentiometry studies were performed for evaluating electrochemical properties using a CHI 660C electrochemistry workstation in a three electrode configuration with $Ni(OH)_2$ loaded Ni foam as the working electrode, platinum foil as the counter electrode and saturated calomel electrode (SCE) as the reference electrode in 2 M KOH solution.

3. Results and discussion

Figure 1 shows X-ray diffraction (XRD) pattern of the as-synthesized $Ni(OH)_2$ nanosheets. The diffraction peaks can be readily indexed as (001), (002), (110), (111) and (300) crystal planes and assigned to the α-$Ni(OH)_2$ structure according to the JCPDS card No. 22-0444. No diffraction peaks from impurities are found in α-$Ni(OH)_2$, indicating that the sample is pure α-$Ni(OH)_2$.

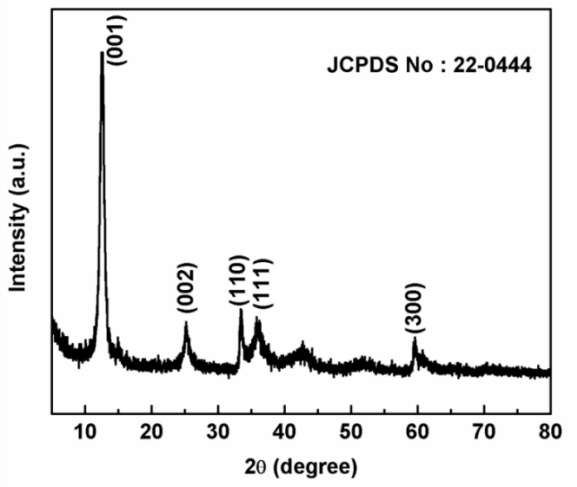

Fig. 1 XRD pattern of α-$Ni(OH)_2$ nanosheets

The $Ni(OH)_2$ nanosheets were characterized by nitrogen adsorption and desorption isotherm and corresponding pore size distribution (as shown in Fig. 2). The isotherm of the $Ni(OH)_2$ nanosheets can be classified as type IV isotherm with a distinct hysteresis loop, reflecting the presence of mesoporous structure .[42] The mesoporous structure was further confirmed by the BJH pore size distribution data. The pore size distribution reveals with a mean pore diameter of 2.9 nm (the inset of Fig. 2). The $Ni(OH)_2$ nanosheets show high BET surface area of 82 m^2 g^{-1}. Generally, increased surface area of electrode/electrolyte interface can enhance the charge transport and improve the electrochemical properties of the electrode. The high BET surface area of $Ni(OH)_2$ nanosheets provide the possibility of effective transportation of electrons and ions, which is very important for electrode materials in practical applications for supercapacitors.

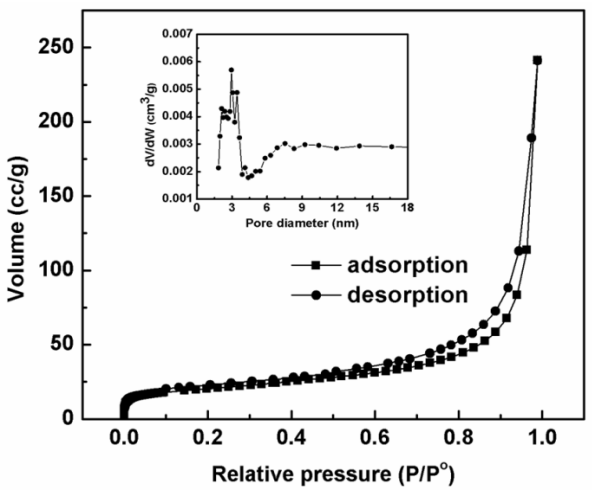

Fig. 2 Nitrogen adsorption/desorption isotherm curve of $Ni(OH)_2$ nanosheets. The inset is the corresponding BJH pore size distributions.

Thermal behaviour of the as-prepared $Ni(OH)_2$ nanosheets was examined by TGA. Figure 3 depicts a typical TGA curve of $Ni(OH)_2$ nanosheets. The initial weight loss from room room temperature to 250 ^oC is about 5 % which is expected to the removal of absorbed water. A very sharp weight loss from 250 ^oC to 310 ^oC suggests the decomposition of $Ni(OH)_2$ to NiO. At

higher temperature there is no major weight loss observed, indicating the absence of additional phase or structural changes.

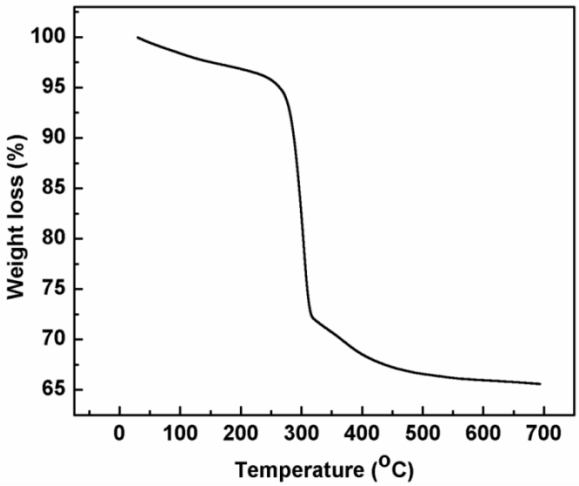

Fig. 3 TGA curve of $Ni(OH)_2$ nanosheets.

The morphology of the $Ni(OH)_2$ nanosheets were observed by FESEM. Figure 4 shows the different magnification SEM images of the as-prepared $Ni(OH)_2$ nanosheets. At the low magnification SEM images (Figure 4(a) and 4(b)) the materials are curely and wrinkled thin sheets of $Ni(OH)_2$. Higher magnification SEM images (Figure 4(c) and 4(d)) reveal that the $Ni(OH)_2$ nanosheets are flexible, interconnected with each other and have an abundant surfaces similar to silk waves.

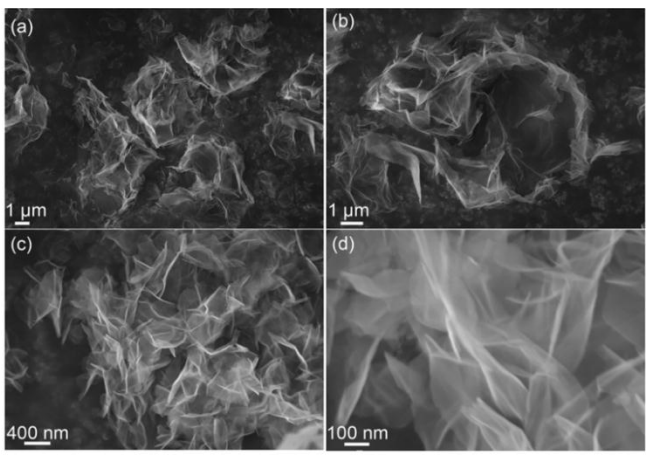

Fig. 4 FESEM images of $Ni(OH)_2$ nanosheets (a) and (b) low magnification and (c) and (d) high magnification.

We used transmission electron microscopy (TEM) to analyse the detailed crystal structure of $Ni(OH)_2$ nanosheets as shown in Figure 5. Figure 5(a) and 5(b) shows the low magnification TEM images of $Ni(OH)_2$ nanosheets, from which it can be seen that the as-prepared $Ni(OH)_2$ present wrinkled paper shape thin sheets. The corresponding selected area electron diffraction (SAED) pattern (Fig. 5(c)) shows the disperse rings were well indexed to the crystal planes of (110), (111), (210), and (221), confirming well crystalline feature of the hexagonal $Ni(OH)_2$. Through the high magnification TEM image (Figure 5(d)) we can observe small pores and the nanosheets demonstrated thin thickness. Fig. 6 shows the atomic force microscopy (AFM) images of $Ni(OH_2$ nanosheets obtained by tapping mode. According to the AFM the thickness of the nanosheets is about 6 nm.

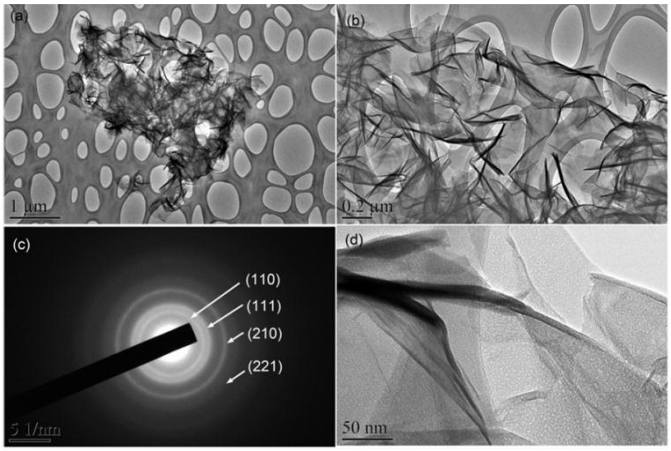

Fig. 5 (a) and (b) Low magnification TEM images of $Ni(OH)_2$ nanosheets. (c) Corresponding selected area electron diffraction pattern (SAED) (d) High magnification TEM image of $Ni(OH)_2$ nanosheets.

The formation mechanism of $Ni(OH)_2$ nanosheets in microwave-mediated process, involves well-known hydrolysis-precipitaion process. In this process, urea generates OH^- ions in the reaction medium, which react with Ni^+ to form $Ni(OH)_2$. The generation of OH^- ions mainly take place at the controlled rate which influences the crystal growth process. The reactions involved in the growth of $Ni(OH)_2$ nanosheets are as follow:[50]

$$NH_2CONH_2 \rightarrow NH_4^+ + NCO^- \quad (1)$$

$$NCO^- + 3H_2O \rightarrow HCO_3^- + NH_4^+ + OH^- \quad (2)$$

$$Ni^+ + 2OH^- \rightarrow Ni(OH)_2 \quad (3)$$

With the existence of ethylene glycol, the product offered nanosheet structure.

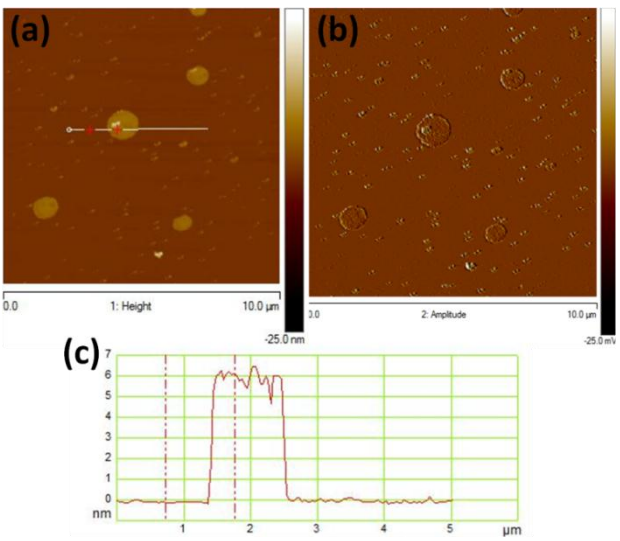

Fig. 6 Atomic force microscopy images of $Ni(OH)_2$ nanosheets obtained by tapping mode. The topography, amplitude and height profile in (a-c) are included, respectively. The height profiles obtained from the topography images are marked by white line with a red cross. Mica discs were used as the substrate.

In this study, we investigated the electrochemical properties of the as-synthesized $Ni(OH)_2$ nanosheets by CV and galvanostatic charge-discharge. Figure 7(a) shows the CV curves of $Ni(OH)_2$ nanosheet electrode at different scan rates in the potential range of 0-0.5 V in 2 M KOH solution. All CV curves comprise a pair of strong redox peaks, which indicates that the capacitance is interrelated with faradic pseudocapacitor. It is apparent that the electron transfer is reversible.[43] The anodic peaks can be observed in the range of 0.3-0.45 V, which are attributed to the reduction of $Ni(OH)_2$ to NiOOH, while the cathodic peaks at 0.1-0.2 V is associated with the conversion of NiOOH back to $Ni(OH)_2$ according to the following reaction mechanism:[44]

$$Ni(OH)_2 + OH^- \leftrightarrow NiOOH + H_2O + e^- \quad (4)$$

The shape of the CV curves does not change expressively, which demonstrates a high electrochemical reactivity.[45] The area under the CV curves can be used to evaluate the capacitance of the system. The specific capacitance values can be calculated from the CV curves by using the following equation:

$$C = Q/\upsilon m\Delta V \quad (5)$$

Where Q is the charge obtained by integrating the CV curves, υ is the scan rate, m is the mass of active material and ΔV is the potential range of each scan. The corresponding specific capacitance is 2351, 2159, 1982, 1742 and 1324 F g^{-1} at the scan rates of 2, 5, 10, 20 and 50 mV s^{-1}, respectively, indicating a high rate capability. The capacitance of the $Ni(OH)_2$ nanosheet electrode was also measured using galvanostatic charge and discharge tests. Figure 7(b) shows the charge-discharge curves of $Ni(OH)_2$ electrode at the current density of 10 A g^{-1} within the voltage range of 0-0.4 V. The shapes of the charge-discharge curves are non-linear, which also clearly demonstrates the pseudo-capacitance of the material. Fig. 8 shows the galvanostatic charge and discharge curves at different current densities. The non-linear charge-discharge curves further verify the pseudo-capacitive properties of $Ni(OH)_2$ nanosheet electrode. The specific capacitance (C) of the $Ni(OH)_2$ electrode was also calculated from the charge-discharge curves according to the equation:

$$C = I\Delta t/\Delta Vm \quad (6)$$

Where I is the discharge current (A g^{-1}), Δt is the discharge time (sec), ΔV is the potential window (V), m is the mass of active material (mg). The specific capacitance calculated from the charge and discharge curves are 2570, 2281, 2105 and 1805 F g^{-1} at the current density of 5, 10, 20 and 40 A g^{-1}, respectively. This indicating the stable reversible features of the nanosheet structure of $Ni(OH)_2$. It is noticeable that the $Ni(OH)_2$ nanosheets can be electrochemically utilized even at high current densities. The amazing improvement of the specific capacitance of $Ni(OH)_2$ nanosheet structure can be ascribed to the effective utilization of layered $Ni(OH)_2$. The interconnected layered thin nanosheet structure (6 nm in thickness) provides adequate space and not only facilitate the penetration of electrolyte into the whole matrix, but also shortens the ion diffusion paths.

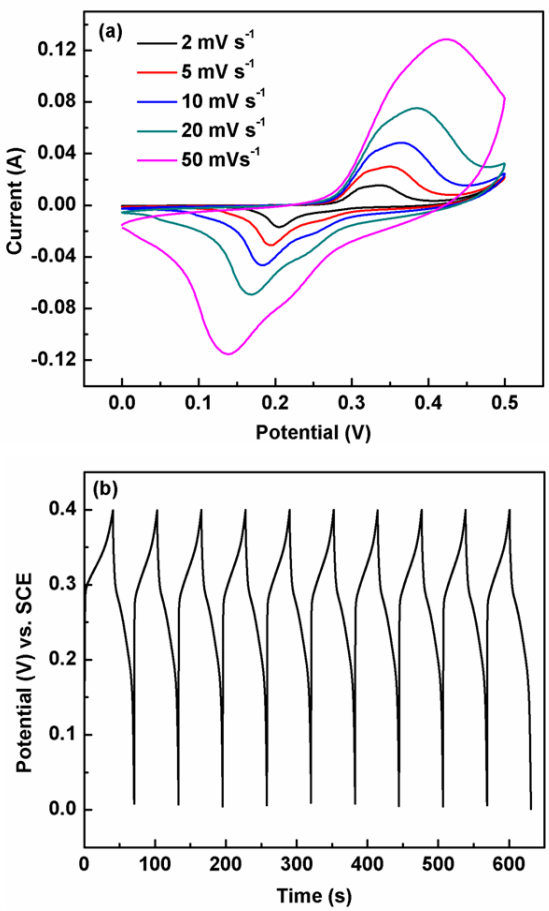

Fig. 7 (a) CV curves of the $Ni(OH)_2$ nanosheet electrode at different scan rates and (b) galvanostatic charge/discharge curves at the current density of 10 A g^{-1} in 2 M KOH electrolyte.

The specific capacitance calculated from both CV and charge-discharge is higher than the previously reported $Ni(OH)_2$ nanoflakes,[46] $Ni(OH)_2$ nanotube arrays[47] and mesoporous $Ni(OH)_2$.[48]

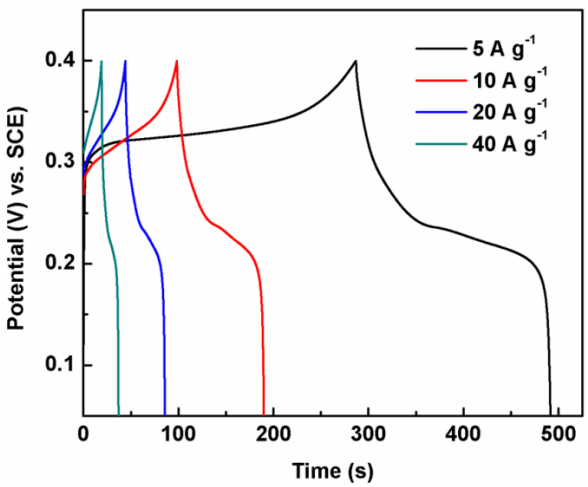

Fig. 8 Galvanostatic charge and discharge curves at different current densities (5 to 40 A g-1)

Figure 9(a) shows the specific capacitances (determined from the CV curves) at different scan rates. The specific capacitance decreased with the increase of scan rates. This can be attributed to the existence of internal active sites that are not able to continue the entire redox conversion at high scan rates, which indicating that some part of the electrode surfaces are not accessible at high scan rates.[49] The long-term cycle stability is the key parameter for pseudocapacitors. As shown in Fig. 9(b) the cycling stability was examined up to 2000 charge-discharge cycles at the scan rate of 50 mV s^{-1} in 2 M KOH electrolyte. The 90 % capacitance is retained after 2000 cycles. The nanosheet structure has many interspaces which can take place the volume expansion easily during charge-discharge cycling, demonstrating an excellent stability of the electrode. In aqueous electrolyte, a little decrease of specific capacitance is observed during long-term charge-discharge cycling, which can be ascribed to the deterioration of active material caused by the partial dissolution in electrolyte and the detachment of active material from the current collector.[51]

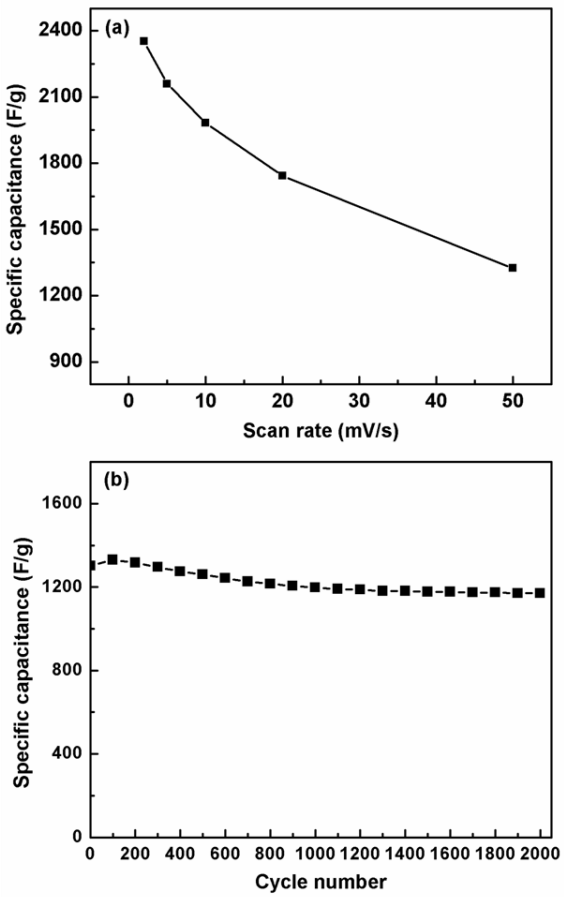

Fig. 9 (a) Specific capacitance as a function of scan rates and (b) cycling performance of $Ni(OH)_2$ nanosheet electrode.

The above results show that the thin $Ni(OH)_2$ nanosheets has high specific capacitance and good cycling stability owing to its thin nanosheet structure with high surface area, indicating an attractive electrode material for supercapacitors.

4. Conclusions

In this work, we synthesized $Ni(OH)_2$ nanosheets through a simple one-step microwave-mediated hydrothermal method. The as-synthesized material has high specific surface area and narrow pore size distribution, which provide more active sites for fast energy storage and also beneficial for the transportation of electrolyte ions. The XRD, BET, SEM, AFM and TEM shows the material is layered thin nanosheet morphology of $Ni(OH)_2$ with mesoporous character. The electrochemical measurements showed that the $Ni(OH)_2$ nanosheets exhibit a high specific capacitance of 2570 F g^{-1} at the current density of 5 A g^{-1} with good cycling stability, suggesting a promising electrode material for supercapacitors.

Acknowledgements

We gratefully acknowledge the financial support provided by the Australian Research Council (ARC) through the ARC discovery project (DP1093855).

Notes and references

[1]Centre for Clean Energy Technology, School of Chemistry and Forensic Science, University of Technology, Sydney, Broadway, Sydney, NSW 2007, Australia.

[2]Institute of Superconducting and Electronic Materials, University of Wollongong, Wollongong, NSW 2522, Australia

E-mail: anjonmondal@yahoo.com, Guoxiu.wang@uts.edu.au

Phone: +61 02 9514 8244

Fax: +61 02 9514 1656

1 R. Kotz and M. Carlen, *Electrochim. Acta*, 2000, **45,** 2483.
2 Y. G. Guo, J. S. Hu and L. J. Wan, *Adv. Mater.*, 2008, **20,** 2878.
3 P. Simon and Y. Gogotsi, *Nat. Mater.*, 2008, **7,** 845.
4 A. Burke, *J. Power Sources*, 2000, **91,** 37.
5 A. S. Arico, P. Bruce, B. Scrosati, J. M. Tarascon and W. V. Schalkwijk, *Nat. Mater.*, 2005, **4**, 366.
6 B. E. Conway, Kluwer Academic/ Plenum Press, New York, 1999.
7 E. Frackowiak and F. Beguin, *Carbon*, 2001, **39,** 937.
8 M. Jayalakshmi and K. Balasubramanian, *Int. J. Electrochem. Sci.*, 2008 **3,** 1196.
9 R. Liu and S. B. Lee, *J. Am. Chem. Soc.*, 2008, **130,** 2942.
10 T. Zhu, J. S. Chen and X. W. Lou, *J. Mater. Chem.*, 2010, **20,** 7015.
11 S. Biswas and L. T. Drzal, *ACS Appl. Mater. Interfaces*, 2010, **2,** 2293.
12 F. Wang, S. Xiao, Y. Hou, C. Hu, L. Liu and Y. Wu, RSC Adv., 2013, **3,** 13059.
13 W. Deng, X. Ji, Q. Chen and C. E. Banks, RSC Adv., 2011, **1,** 1171.
14 H. S. Kim and B. N. Popov, *J. Power Sources*, 2002, **104,** 52.
15 L. Wang, X. H. Liu, X. Wang, X. J. Yang and L. D. Lu, *Curr. Appl. Phys.*, 2010, **10,** 1422.
16 H. S. Nam, J. S. Kwon, K. M. Kim, J. M. Ko and J. D. Kim, *Electrochim. Acta*, 2010, **55,** 7443.
17 Q. Qu, P. Zhang, B. Wang, Y. Chen, S. Tian, Y. Wu and R. Holze, J. Phys. Chem. C, 2009, **113,** 14020.
18 P. Justin, S. K. Meher and G. R. Rao, *J. Phys. Chem. C*, 2010, **114,** 5203.
19 S. Chen, J. Zhu and X. Wang, *J. Phys. Chem. C*, 2010, **114,** 11829.
20 Y. F. Liu, H. G. Pan, M. X. Gao and Q. D. Wang, *J. Mater. Chem.*, 2011, **21,** 4743.
21 B. Hariprakash, S. K. Martha, M. S. Hegde and A. K. Shukla, *J. Appl. Electrochem.*, 2005, **35,** 27.
22 A. K. Shukla, S. Venugopalan and B. Hariprakash, *J. Power Sources*,

2001, **100,** 125.
23 L. X. Lei, M. Hu, X. R. Gao and Y. M. Sun, *Electrochim. Acta*, 2008, **54,** 671.
24 Y. Yuan, X. Xia, J. Wu, J. Yang, Y. Chen and S. Guo, *Electrochim. Acta*, 2011, **56,** 2627.
25 H. Wang, H. S. Casalongue, Y. Liang and H. Dai, *J. Am. Chem. Soc.*, 2010, **132,** 7472.
26 G. Hu, C. Li and H. Gong, *J. Power Sources*, 2010, **195,** 6977.
27 C. Y. Yan, H. Jang, T. Zhao, C. Z. Li, J. Ma and P S. Lee, *J. Mater. Chem.*, 2011, **21,** 10482.
28 J. W. Xiao and S. H. Yang, *RSC Adv.*, 2011, **1,** 588.
29 S Chen, J. W. Zhu, H. Zhou and X. Wang, *RSC Adv.*, 2011, **1,** 484.
30 S. K. Meher, P. Justin and G. R. Rao *Nanoscale*, 2011, **3,** 683.
31 C. Coudun, F. Grillon and J. F. Hochepied, *Colloids Surf. A*, 2006, **280,** 23.
32 B. Mavis and M. Akine, *Chem. Mater.*, 2006 **18**, 5317.
33 M. Aghazadeh, A. N. Golikand and M. Ghaemi, *Int. J. Hydrogen Energy*, 2011, **36,** 8674.
34 D. P. Dubal, V. J. Fulari and C. D. Lokhande, *Microporous Mesoporous Mater.*, 2012, **151** 511.
35 Y. X. Wang, Z. A. Hu and H. Y. Wu, *Mater. Chem. Phys.*, 2011 **126,** 580.
36 L. Gong, X. Liu and L. Su *J. Inorg. Oganomet. Polym.*, 2011 **21,** 866.
37 J. Liu, S. Du, L. Wei, H. Liu, Y. Tian and Y. Chen, *Mater. Lett.*, 2006, **60,** 3601.
38 C. Yuan, X. Zhang, L. Su, B. Gao and L. Shen, *J. Mater. Chem.*, 2009, **19,** 5772.
39 I. Bilecka and M. Niederberger, *Nanoscale*, 2010, **2,** 1358.
40 G. A. Tompsett, W. C. Conner and K. S. Yngvesson, *Chem. Phys. Chem.*, 2006, **7,** 296.
41 V. Polshettiwar, B. Baruwati and R. S. Varma, *ACS Nano*, 2009, **3,** 728.
42 A. Vinu, D. P. Sawant, K. Ariga, M. Hartmann and S. B. Halligudi, Microporous Mesoporous Mater., 2005, 80, 195.
43 Y. Y. Liang, S. J. Bao and H. L. Li, *J. Solid State Electrochem.*, 2007, **11,** 571.
44 W. Zhou, M. Yao, L. Guo, Y. Li, J. Li, and S. Yang, *J. Am. Chem. Soc.*, 2009, **131,** 2959.
45 Y. Y. Liang, M. G. Schwab, L. J. Zhi, E. Mugnaioli, U. Kolb, X. L. Feng and K. Mullen, *J. Am. Chem. Soc.*, 2010, **132,** 15030.
46 J. W. Lang, L. B. Kong, W. J. Wu, M. Liu, Y. C. Luo and L. Kang, *J. Solid State Electrochem.*, 2009, **13,** 333.
47 M. Sung and K. C. Huang, *Chem. Commun.*, 2011, **47,** 12122.
48 S. Xing, Q. Wang, Z. Ma, Y. Wu and Y. Gao, *Mater. Lett.*, 2012 **78,** 99.
49 U. M. Patil, K. V. Gurav, V. J. Fulari, C. D. Lokhande and O. S. Joo *J. Power Sources*, 2009, **188,** 338.,
50 M. Rose, W. Bohlmann, M. Sabo and S. Kaskel, Chem. Commun., 2008, **11,** 2462.
51 D. S. Dhawale, R. R. Salunkhe, V. S. Jamadade, D. P. Dubal, S. M. Pawar and C. D. Lokhande, Curr. Appl. Phys., 2010, 10, 904.

Table of content (TOC)

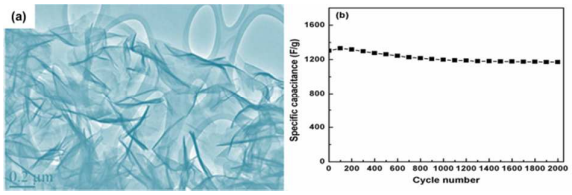

Text: A simple microwave-assisted synthesis of $Ni(OH)_2$ nanosheets for supercapacitors with high specific capacitance and superior cycling stability